

Mn abundances in the stars of the Galactic disc with metallicities $-1.0 < [\text{Fe}/\text{H}] < 0.3$ * †

T. Mishenina¹, T. Gorbaneva¹, M. Pignatari^{2,3,4}, F.-K. Thielemann³,
S.A. Korotin¹

¹ *Astronomical Observatory, Odessa National University, and
Isaac Newton Institute of Chile, Odessa branch, Shevchenko Park, 65014, Odessa, Ukraine*

² *Konkoly Observatory, Research Centre for Astronomy and Earth Sciences, Hungarian Academy of Sciences,
Konkoly Thege Miklos ut 15-17, H-1121 Budapest, Hungary*

³ *Department of Physics, University of Basel, Klingelbergstrabe 82, 4056 Basel, Switzerland*

⁴ *The NuGrid collaboration, <http://www.nugridstars.org>*

Accepted 2015 xxx. Received 2015 xxx; in original form 2015 xxx

ABSTRACT

In this work we present and discuss the observations of the Mn abundances for 247 FGK dwarfs, located in the Galactic disc with metallicity $-1 < [\text{Fe}/\text{H}] < +0.3$. The observed stars belong to the substructures of the Galaxy thick and thin discs, and to the Hercules stream. The observations were conducted using the 1.93 m telescope at Observatoire de Haute-Provence (OHP, France) equipped with the echelle type spectrographs ELODIE and SOPHIE. The abundances were derived under the LTE approximation, with an average error for the $[\text{Mn}/\text{Fe}]$ ratio of 0.10 dex. For most of the stars in the sample Mn abundances are not available in the literature. We obtain an evolution of $[\text{Mn}/\text{Fe}]$ ratio with the metallicity $[\text{Fe}/\text{H}]$ consistent with previous data compilations. In particular, within the metallicity range covered by our stellar sample the $[\text{Mn}/\text{Fe}]$ ratio is increasing with the increase of metallicity. This due to the contribution to the Galactic chemical evolution of Mn and Fe from thermonuclear supernovae. We confirm the baseline scenario where most of the Mn in the Galactic disc and in the Sun is made by thermonuclear supernovae. In particular, the effective contribution from core-collapse supernovae to the Mn in the Solar system is about 10-20%. However, present uncertainties affecting the production of Mn and Fe in thermonuclear supernovae are limiting the constraining power of the observed $[\text{Mn}/\text{Fe}]$ trend in the Galactic discs on, e.g., the frequency of different thermonuclear supernovae populations. The different production of these two elements in different types of thermonuclear supernovae needs to be disentangled by the dependence of their relative production on the metallicity of the supernova progenitor.

Key words: stars: abundances – stars: late-type – Galaxy: disc – Galaxy: evolution

1 INTRODUCTION

Manganese (Mn, $Z=25$) is a monoisotopic element member of the iron group. In stellar spectra several Mn absorption lines are known. Since early studies of stellar chemical composition, it was observed that in metal-poor stars Mn has a different behaviour with respect to Fe compared to other iron-peak elements. (e.g., Wallerstein 1962). The chemical evolution of $[\text{Mn}/\text{Fe}]$ is also different compared to

α -elements (O, Mg, Si, S, Ca and Ti), which abundances increase with the metallicity decreasing (e.g., Gratton 1989).

Today a large number of Mn spectroscopic observations are available for stars with different age and metallicity and from different galactic hosts, e.g., from our Galaxy, from Globular Clusters (GCs) including Omega-Cen, and from Dwarf Spheroidal Galaxies (e.g., Prochaska et al. 2000; McWilliam, Rich & Smecker-Hane 2003; Alves-Brito, Barbuy & Allen 2007; Sobeck et al. 2006; Cunha et al. 2010; Pancino et al. 2011). In particular, the Mn abundance survey in globular clusters and field stars within the metallicity range $-2.7 < [\text{Fe}/\text{H}] < -0.7$ by Sobeck et al. (2006) found consistent average $[\text{Mn}/\text{Fe}]$

* Based on observations collected at OHP observatory, France

† Table 1 are only available in electronic form

ratios ($[\text{Mn}/\text{Fe}] = -0.36$ and -0.37 , respectively) for those two populations. This is consistent with the fact that for metallicities $[\text{Fe}/\text{H}] \lesssim -1$ core-collapse supernovae (CCSNe) are the only astrophysical producers of Mn in the Galaxy (e.g., Thielemann, Nomoto & Hashimoto 1996; Woosley, Heger & Weaver 2002; Nomoto, Kobayashi & Tominaga 2013). The same is true for GCs, where the mass of the cluster is not large enough to keep the supernovae ejecta, and all Mn and Fe observed is due to pollution from massive stars before the GC formed. This is the main reason for the good agreement for the average $[\text{Mn}/\text{Fe}]$ observed in unevolved halo stars and in GCs (Sobeck et al. 2006). On the other hand, the star-to-star scatter reported by Sobeck et al. (2006) is $-0.6 \lesssim [\text{Mn}/\text{Fe}] \lesssim 0$, that is larger than the reported observational errors. The same conclusion may be derived by the observation in halo stars ($-1.1 \lesssim [\text{Mn}/\text{Fe}] \lesssim 0.5$) and from Omega Cen ($-0.8 < [\text{Mn}/\text{Fe}] < -0.2$, Cunha et al. 2010; Pancino et al. 2011). Such a large spread is difficult to reconcile with baseline one-dimensional CCSN models (e.g., Woosley & Weaver 1995; Limongi, Straniero & Chieffi 2000), where for an amount of ^{56}Ni ejected in the order of $0.1 M_{\odot}$ the stellar yields show an $[\text{Mn}/\text{Fe}]$ ratio $\gtrsim -0.5$. Therefore, the origin of the $[\text{Mn}/\text{Fe}]$ in the range $-1.0 \lesssim [\text{Mn}/\text{Fe}] \lesssim -0.5$ is not clearly understood (Andrievsky, Korotin & Martin 2007), although an increase of Y_e in the ejecta (see Fig. 5 in Thielemann, Nomoto & Hashimoto 1996), as expected from neutrino interactions (see Fröhlich et al. 2006) can explain smaller values. An alternative scenario, in order to reproduce the low $[\text{Mn}/\text{Fe}]$ ratio is the contribution from Hypernovae, ejecting large quantities of Fe compared to Mn (e.g., Umeda & Nomoto 2005; Nomoto et al. 2006; Nomoto, Kobayashi & Tominaga 2013).

The observation of Mn abundances may be affected by deviations from the LTE. Bergemann & Gehren (2008) have found that $[\text{Mn}/\text{Fe}]$ ratio measured in LTE approximation might underestimate the real Mn abundances up to 0.5–0.6 dex for the metal-poor stars, and ~ 0.1 dex for stars of solar-like metallicities.

For metallicities higher than $[\text{Fe}/\text{H}] \sim -1$ typical of the Galactic discs, the observation of the $[\text{Mn}/\text{Fe}]$ ratio is still controversial. Nissen et al. (2000) and Reddy, Lambert & Allende Prieto (2006) reported similar Mn abundance trends with $[\text{Fe}/\text{H}]$ for thick and thin disc stars. On the other hand, Feltzing, Fohlman & Bensby (2007) and Battistini & Bensby (2015) found a different behaviour in the two stellar populations. A similar result is obtained by Hawkins et al. (2015) for giant stars.

The nucleosynthesis of Mn becomes more complex for metallicities typical of the Galactic disc. Thermonuclear supernovae (SNIa, e.g., Hillebrandt et al. 2013, for a recent review) start to contribute to the production of Mn and Fe for $[\text{Fe}/\text{H}] \gtrsim -1$ (Matteucci & Greggio 1986), leading to the observed increasing trend of $[\text{Mn}/\text{Fe}]$ up to the present solar values. In particular, most of the Fe and Mn observed today in the Solar system are made by SNe Ia (e.g., Timmes, Woosley & Weaver 1995; Cescutti et al. 2008; Kobayashi, Karakas & Umeda 2011). The production of Fe in SNe Ia as ^{56}Ni is not completely independent from the initial metallicity of the star, and its production tends to decrease with

the increasing metallicity (Timmes, Brown & Truran 2003; Travaglio, Hillebrandt & Reinecke 2005; Bravo et al. 2010). On the other hand, Mn production increases with the initial metallicity of the SNIa progenitor (e.g., Iwamoto et al. 1999; Travaglio, Hillebrandt & Reinecke 2005), which is consistent with the increasing $[\text{Mn}/\text{Fe}]$ with $[\text{Fe}/\text{H}]$. The metallicity dependence of Mn production in SNe Ia was also inferred by Galactic chemical evolution (GCE) simulations (Cescutti et al. 2008).

One of the main uncertainties affecting the evolution of Mn abundance in the Galactic disc is our present understanding of SNIa nucleosynthesis. The two historical scenarios proposed for SNe Ia are the single-degenerate scenario (SDS), where an accreting white dwarf (WD) is reaching the Chandrasekhar mass by accreting material from a stellar binary companion, or the double-degenerate scenario (DDS), where a SNIa is formed by a merger of two CO WDs. Based on different motivations, in the last decades one or the other scenario have been favoured (see discussion in Hillebrandt et al. 2013). Another scenario related to the SDS is the double-detonation SN, where the SNIa explosion is triggered by the He detonation initiated in the external He shell during the accretion on a sub-Chandrasekhar progenitor (Pakmor et al. 2010; Fink et al. 2010).

Based on GCE calculations of the $[\text{Mn}/\text{Fe}]$ ratio in the Galactic disc, Matteucci et al. (2009) proposed that two different types of SNIa contributors are needed to reproduce the observations. More recently, based on the use of stellar yields from multi-dimensional hydrodynamics simulations of SNe Ia, Seitzzahl et al. (2013a) confirmed that both SNIa scenarios with a mass close to the Chandrasekhar limit and with sub-Chandrasekhar mass (i.e., DDS or double-detonation in an accreting sub-Chandrasekhar progenitor) are needed to fit the $[\text{Mn}/\text{Fe}]$ evolution. In particular, the yields of the first ones carry a much larger Mn/Fe ratio than the second ones.

In this work we provide the measurement for Mn abundances for 247 F-G-K-type dwarf stars located in the thin and thick disc populations, and for the Hercules Stream, covering the metallicity range $-1.0 < [\text{Fe}/\text{H}] < 0.3$. The main purpose of this survey is to provide new constraints helping to definitely establish the origin of the Mn production in the Galactic disc. The paper is organized as follow. The observations and selection of stars, and definition of the main stellar parameters are described in §2. The abundance determinations for Mn and the error analysis are presented in §3. In §4 the results are compared with other measurements available in the literature. The implications of the results and the nucleosynthesis of Mn in stars is reported in §5. Conclusions are drawn in §6.

2 OBSERVATIONS, SELECTION AND PARAMETERS OF THE DISC STARS

The investigated stellar spectra were obtained using the 1.93 m telescope at Observatoire de Haute-Provence (OHP, France) equipped with echelle type spectrographs, namely SOPHIE, resolving power $R = 75\,000$ (Perruchot et al. 2008) and ELODIE, $R = 42\,000$ (Baranne et al. 1996), in the wavelength range $\lambda 4400\text{--}6800 \text{ \AA}$ and signal-to-noise ratio of about 100–300.

To distinguish between stars in the thin disc, thick disc and the Hercules Stream, we considered the probability that a star belongs to either one of them accounting for its spatial velocity, kinematic disc parameters, and the quantity and percentage of every disc stars in our sample. The stars that belong to the Galactic sub-structures were selected using the technique described in Mishenina et al. (2004). The primary processing of spectra was carried out immediately during observations (Katz et al. 1998). Further spectra processing such as the continuum placement, line depth and equivalent width (EW) measurements, etc., was conducted using the DECH20 software package by Galazutdinov (Galazutdinov G. A. 1992). The atmospheric parameters of target stars has been determined earlier. The methods applied are described in detail in Mishenina & Kovtyukh (2001), Mishenina et al. (2004) and Mishenina et al. (2008).

The effective temperatures T_{eff} are defined by calibration of line-depth ratios (R1/R2) for spectral line pairs that markedly differ in their low-level excitation potential Kovtyukh et al. (2003). A large number of calibrations (80–103) permitted to reduce the influence of errors in the line-depth and atmospheric parameter measurements on the resulting temperature estimates. The intrinsic accuracy of the method applied for dwarfs is 5–45 K. For the stars with $[\text{Fe}/\text{H}] < -0.5$ the T_{eff} were estimated by adjustment of far-wings of the H_α line (Mishenina & Kovtyukh 2001).

The surface gravities $\log g$ values are computed by the ionization balance of the neutral and ionized iron. This method implies that similar abundances are obtained from the neutral iron FeI and ionized iron FeII lines. Its accuracy is affected by a number of factors, such as uncertainty of oscillator strengths of the $\log gf$ lines and thermal structure of atmospheric models, and NLTE effects.

However, the determination of the surface gravity by the parallax method is also affected by uncertainties. In order to determine the stellar mass by using theoretical evolution tracks, it is necessary to measure in advance the metallicity and α -element enrichment, leading to an uncertainty in the mass determination of $\sim 0.2M_\odot$, which corresponds to an error for the surface gravity of ~ 0.1 dex. Therefore, NLTE effects and atmospheric model uncertainties still affect the analysis. As reported by Allende Prieto et al. (1999), the astrometric and spectroscopic methods provide consistent results in the metallicity range $-1 < [\text{Fe}/\text{H}] < 0.3$. Having compared the resulting $\log g$ obtained by us using the ionization balance method with the $\log g$ value computed by using the parallax in Allende Prieto et al. (1999) for 39 stars in common, leads to differences not exceeding 0.1 dex on average Mishenina et al. (2004).

The microturbulence velocity V_t is derived considering that the iron abundance obtained from the given FeI line is not correlated with the equivalent width EW of that line. The adopted value of metallicity $[\text{Fe}/\text{H}]$ is the iron abundance derived from the FeI lines. The determination errors are: for the effective temperatures $\delta T_{\text{eff}} = \pm 100\text{K}$, the surface gravities $\delta \log g = \pm 0.2\text{dex}$, the microturbulence velocity $\delta V_t = \pm 0.2\text{km/sec}$. The obtained parameter values and their comparison with the results of other authors are reported in Mishenina et al. (2004) and Mishenina et al. (2013).

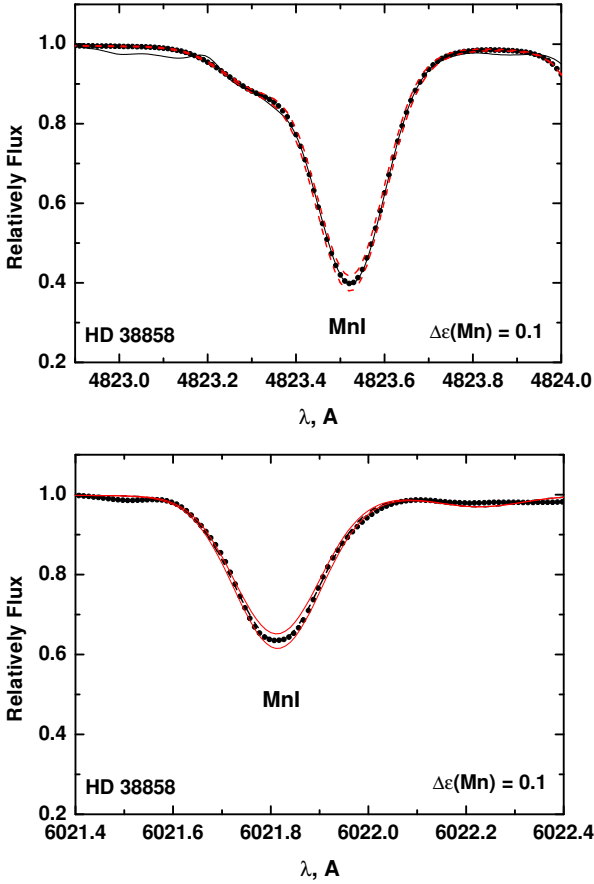
3 THE MN ABUNDANCE

The Mn abundances were derived by computing the synthetic spectrum in the region of the Mn lines by the newly updated STARS LTE software (Tsymbal 1996) using the Kurucz models (Castelli & Kurucz 2004). The MnI lines undergo hyperfine-structure (HFS) splitting, due to the interaction of the magnetic moment of the nucleus with the magnetic field of the electrons. The list of lines and HFS data were taken from Prochaska et al. (2000). The van der Waals damping constant C_6 was taken from Bergemann & Gehren (2008). Atomic data for other lines required to compute the synthetic spectrum in the region of the MnI lines were taken from the Vienna Atomic Line Database VALD (Kupka et al. 1999). The solar MnI abundances are derived for each line by the solar spectra reflected by the moon and asteroids. Two echelle type spectrographs were adopted. In order to select reliable fitting lines, we started with derivation of the Mn abundances from 16 MnI lines in the atmospheres of the Sun and some other stars, using spectra obtained with both spectrographs. A total of 6 solar spectra were used, including three spectra obtained with the echelle type spectrograph ELODIE and three spectra received by the echelle type spectrograph SOPHIE. Five lines were obtained: 4783, 4823, 5432, 6013 and 6021 Å. The equivalent widths EWs averaged by spectra for each spectrograph differ by 1–2% for strong lines and 2–3% for the 5432 Å line. The mean difference of EWs of Mn lines in spectra obtained with two spectrographs is $\langle (\text{EWs}(\text{Mn})_{\text{SOPHIE}} - \text{EWs}(\text{Mn})_{\text{ELODIE}}) \rangle = -1.8 \pm 0.7 \text{ m}\text{\AA}$. Further, we also compared of EWs of Fe I lines measured in solar spectra obtained with two spectrographs. The mean difference in this case is $\langle (\text{EWs}(\text{Fe})_{\text{SOPHIE}} - \text{EWs}(\text{Fe})_{\text{ELODIE}}) \rangle = -1.2 \pm 2.3 \text{ m}\text{\AA}$. Hence, the MnI abundance derived from selected lines in the solar spectra obtained with both spectrographs are consistent. Lines 4783 and 4823 Å are rather strong, so they were not used in the analysis of cooler stars ($T_{\text{eff}} < 5200 \text{ K}$) and those more enriched in iron ($[\text{Fe}/\text{H}] > 0$). For each line we derived the Mn abundances in the solar and stellar spectra, by fitting locally the observed spectra with the synthetic model. For a given line we compare the abundance value to the solar abundance. We adopted this differential approach to eliminate the impact of potential errors in the oscillator strengths led to the following adopted atomic parameters. Finally, we derived the stellar Mn abundance by averaging the values obtained for each line (Table 1). The mean solar abundance computed for the lines with $\log gf$ from VALD data base (Kupka et al. 1999) and the solar model from Castelli & Kurucz (2004) and adopted values for each line in this work are 5.3, 5.25, 5.27, 5.24, and 5.24 for the lines λ 4783, 4823, 5432, 6013, 6021 Å, respectively. In Fig. 1 we show few examples of profile fitting for Mn lines.

For a sample of stars also analysed by other studies, we compare the inferred atmospheric parameters in Table 2. Impact of these variations are within the observational errors for Mn abundance. For a detailed comparison we show in Table 3 the stellar data for each star together with other works. Takeda (2007) and Nissen & Schuster (2011) show the largest variations compared to our T_{eff} , but they also report larger errors ($\sigma \gtrsim 100 \text{ K}$). The biggest departure is for HD 4307 by Takeda (2007), with a difference for T_{eff} larger than 200 K. In the Table 4 we presented the comparison of

Table 1. Atmospheric parameters and Mn abundance $\log A(\text{Mn})$ each used line (λ , Å) and $[\text{Mn}/\text{Fe}]$ ratio for our target stars

Star	$T_{\text{eff},\text{K}}$	$\log g$	$[\text{Fe}/\text{H}]$	Vt	4783 Å	4823 Å	5432 Å	6013 Å	6021 Å	$[\text{Mn}/\text{Fe}]$
Sun					5.30	5.25	5.27	5.24	5.24	
Thick disc										
HD245	5400	3.4	-0.84	0.7	4.32	4.35	4.10	4.18	4.18	-0.16
HD3765	5079	4.3	0.01	1.1			5.30	5.30	5.30	0.04
HD6582	5240	4.3	-0.94	0.7	4.20	4.20	4.18	4.15	4.15	-0.14
HD13783	5350	4.1	-0.75	1.1	4.35	4.40	4.40		4.25	-0.17
HD18757	5741	4.3	-0.25	1.0	4.95	4.95	4.95	4.85	4.85	-0.10
...
...
...

**Figure 1.** Example of the fitting of the observed spectrum (black dots with solid line) by the synthetic spectrum (red dotted line) in the area of the Mn lines.

the data of Battistini & Bensby (2015) and our determinations of parameters and Mn abundance for common stars. A good agreement is obtained between these two data sets.

3.1 Errors in abundance determinations

To determine the systematic errors in the Mn abundance resulting from uncertainties in the atmospheric parameter determinations, we derived the Mn abundance for several models with modified parameters ($\delta T_{\text{eff}} = \pm 100 \text{ K}$, $\delta \log g = \pm 0.2$, $\delta Vt = \pm 0.1$). The Mn abundance variations with the modi-

Table 5. Abundance uncertainties due to atmospheric parameters.

Mn I lines	$\Delta T_{\text{eff}+}$	$\Delta \log g+$	$\Delta Vt+$	tot+
	HD 22879 (5972/4.5/1.1/-0.77)			
4783	-0.08	0.02	0.03	
4823	-0.08	0.01	0.02	
5432	-	-	-	
6013	-0.06	0.02	0.02	
6021	-0.06	0.02	0.01	
average	-0.07	0.017	0.02	0.08
	HD 26923 (5920/4.4/1.0/-0.03)			
4783	-0.06	0.03	0.03	
4823	-0.07	0.01	0.02	
5432	-0.08	0.02	0.03	
6013	-0.05	0.02	0.03	
6021	-0.06	0.02	0.01	
average	-0.06	0.02	0.02	0.08
	HD 4635 (5103/4.4/0.8/0.07)			
4783	-0.10	0.04	0.02	
4823	-0.10	0.05	0.02	
5432	-0.08	0.03	0.06	
6013	-0.06	0.05	0.02	
6021	-0.04	0.05	0.04	
average	-0.08	0.04	0.03	0.10

fied parameters and the fitting errors for the computed and observed spectral line profiles (0.03 dex), are given in Table 5. The largest error occurs when the T_{eff} are determined inaccurately. Errors caused by uncertainties from other parameters are marginal. The total error associated with the determination of the Mn abundances is 0.08 – 0.10 dex (Table 5.)

The graph of plotted points corresponding to the Mn abundances for each line in spectra of all investigated stars is presented in Fig. 2. In particular, there is no systematic difference in abundances obtained for a given line. The correlation between $\sigma([\text{Mn}/\text{H}])$ and $[\text{Mn}/\text{H}]$, where σ is the standard deviation, the mean value of which is 0.03, is shown in Fig. 2. No trend is observed on the graph of $\sigma([\text{Mn}/\text{H}])$ dependence on T_{eff} , $\log g$ or $[\text{Fe}/\text{H}]$ either (Fig. 2).

Table 2. Comparison of our parameters and Mn abundance determinations with the results of other authors for the n stars shared with our stellar sample.

	$\Delta(T_{\text{eff}})$	$\Delta(\log g)$	$\Delta([\text{Fe}/\text{H}])$	$\Delta([\text{Mn}/\text{Fe}])$	n
Feltzing et al.	24	-0.03	-0.01	0.02	10
2007	± 76	± 0.13	± 0.08	± 0.06	
Reddy et al.	105	-0.18	0.01	0.14	9
2006	± 100	± 0.21	± 0.11	± 0.06	
Takeda	-14	-0.06	-0.04	0.02	31
et al. 2007	± 119	± 0.21	± 0.10	± 0.08	
Nissen et al.	7	-0.03	-0.05	0.02	4
2011	± 143	± 0.20	± 0.10	± 0.02	
Adibekyan	28	-0.07	0.01	0.01	9
et al. 2014	± 57	± 0.14	± 0.04	± 0.05	
Battistini & Bensby	-4	-0.10	-0.03	0.02	22
2015	± 106	± 0.15	± 0.06	± 0.06	

Table 3. Comparison of atmospheric parameters and Mn abundance for common stars.

HD	sources	T_{eff}	$\log g$	[Fe/H]	[Mn/Fe]
4307	Adibekyan et al. 2012	5812	4.10	-0.23	-0.07
	Takeda 2007	5648	3.75	-0.29	-0.09
	our	5889	4.00	-0.18	-0.06
6582	Reddy et al. 2006	5300	4.67	-0.86	-0.23
	Takeda 2007	5330	4.54	-0.81	-0.12
	our	5240	4.30	-0.94	-0.14
22879	Adibekyan et al. 2012	5884	4.52	-0.82	-0.30
	Feltzing et al. 2007	5920	4.33	-0.84	-0.18
	Nissen&Shuster 2011	5759	4.25	-0.85	-0.27
	Reddy et al. 2006	5722	4.50	-0.87	-0.39
	our	5972	4.50	-0.77	-0.22
76932	Feltzing et al. 2007	5875	4.10	-0.91	-0.23
	Nissen&Shuster 2011	5877	4.13	-0.87	-0.25
	Reddy et al. 2006	5783	4.09	-0.86	-0.35
	our	5840	4.00	-0.95	-0.25
106516	Nissen&Shuster 2011	6196	4.42	-0.68	-0.23
	Reddy et al. 2006	6069	4.44	-0.74	-0.35
	our	6165	4.40	-0.72	-0.23
125184	Adibekyan et al. 2012	5680	4.10	0.27	0.06
	Takeda 2007	5629	4.02	0.25	0.24
	our	5695	4.30	0.31	0.02
157214	Reddy et al. 2006	5605	4.49	-0.41	-0.24
	Takeda 2007	5693	4.21	-0.37	-0.15
	our	5820	4.50	-0.29	-0.11
159482	Nissen&Shuster 2011	5737	4.31	-0.73	-0.23
	Reddy et al. 2006	5630	4.58	-0.70	-0.32
	our	5620	4.10	-0.89	-0.21
199960	Adibekyan et al. 2012	5973	4.39	0.28	0.10
	Feltzing et al. 2007	5924	4.26	0.28	0.23
	Takeda 2007	5924	4.26	0.28	-0.04
	our	5878	4.20	0.23	0.02
217014	Feltzing et al. 2007	5789	4.34	0.20	0.02
	Takeda 2007	5779	4.31	0.20	-0.09
	our	5763	4.30	0.17	0.00

3.2 Analysis of the Mn spectral line parameters and evaluation of the effects of deviations from LTE on determination of the Mn abundance.

In order to analyse and compare consistently the Mn abundance obtained in different works, it is necessary to take into

account that the authors used different oscillator strengths $\log gf$ and different atomic data to account for HFS in their analysis. The values of the NLTE corrections for the Mn lines, including those used in our study, are investigated by Bergemann & Gehren (2007) and Bergemann & Gehren (2008). The difference in the NLTE corrections change for different lines and depends on temperature and metallicity

Table 4. Comparison of atmospheric parameters and Mn abundance for common stars with Battistini & Bensby (2015) (BB 2015).

HIP	HD	T_{eff} BB 2015	$\log g$	[Fe/H]	[Mn/Fe]	T_{eff} our	$\log g$	[Fe/H]	[Mn/Fe]
6653	8648	5841	4.3	0.22	0.02	5790	4.2	0.12	0.02
16852	22484	6036	4.1	-0.03	-0.07	6037	4.1	-0.03	-0.04
17147	22879	5970	4.5	-0.81	-0.3	5972	4.5	-0.77	-0.22
22263	30495	5790	4.5	0.02	-0.18	5820	4.4	-0.05	-0.03
30545	45067	6042	3.9	-0.03	-	6058	4	-0.02	-0.09
38625	64606	5188	4.4	-0.91	-0.08	5250	4.2	-0.91	-0.11
38750	64815	5763	3.9	-0.35	-0.19	5864	4	-0.33	-0.14
44075	76932	5937	4.2	-0.9	-	5840	4	-0.95	-0.24
64792	115383	6185	4.3	0.25	0.02	6012	4.3	0.11	0.00
74537	135204	5200	4.4	-0.19	-	5413	4	-0.16	-0.03
81300	149661	5216	4.6	-0.01	-	5294	4.5	-0.04	-0.03
82588	152391	5322	4.5	-0.08	-	5495	4.3	-0.08	0.05
84905	157089	5915	4.3	-0.5	-	5785	4	-0.56	-0.19
86013	159482	5760	4.3	-0.81	-0.18	5620	4.1	-0.89	-0.21
86193	159909	5671	4.3	0.03	-0.07	5749	4.1	0.06	0.00
88622	165401	5794	4.5	-0.4	-0.16	5877	4.3	-0.36	-0.09
93966	178428	5656	4.2	0.15	-0.04	5695	4.4	0.14	0.00
97779	187897	5944	4.5	0.12	-0.03	5887	4.3	0.08	-0.02
98767	190360	5572	4.5	0.26	-	5606	4.4	0.12	0.05
103682	199960	6023	4.4	0.33	0.08	5878	4.2	0.23	0.02
104659	201891	5973	4.3	-1.08	-0.26	5850	4.4	-0.96	-0.28
113357	217014	5858	4.4	0.24	0.02	5763	4.3	0.17	0.00

(Bergemann & Gehren 2008). The obtained variations for lines of various multiplets often exceed 0.10 dex. Therefore, the LTE Mn abundances obtained from the lines of different multiplets must show systematic variations between them. According to Bergemann & Gehren (2008) due to the NLTE effects we should have obtained the systematic difference in LTE Mn abundance for two line groups of different multiplets. We used pairs of the lines 4783–4823 Å (multiplet 16, $E_{\text{low}} = 2.3$ eV) and 6013–6021 Å (multiplet 27, $E_{\text{low}} = 3.07$ eV). In Figs. 3, 4 we show the dependences of the difference in abundances $\Delta \text{Log} A = \text{Log} Mn_{4783} - \text{Log} Mn_{6013}$ on the effective temperature and metallicity for the thin and thick disc stars. There is no systematic trend observed. The average variations are 0.01 ± 0.04 and 0.02 ± 0.04 for the thin and thick discs, respectively. Thus, the observations do not support the values of the LTE deviations obtained by Bergemann & Gehren (2008) at the given temperatures and metallicities.

The development of an adequate model of Mn atoms to account for the effects of deviations from LTE is complicated by the absence of detailed computations of atomic data, such as photoionization cross-section or parameters of radiative and shock transitions. The use of approximations such as a H-like approximation for Mn atoms, yields NLTE corrections that are not robust. Taking all this into account, we believe instead that the LTE determinations for the Mn abundance are correct within the given uncertainty of 0.1 dex.

4 RESULTS AND COMPARISON WITH THE LITERATURE.

The Mn abundances obtained for our stellar sample is shown in Fig. 5, upper panel. In Figure 6 our results are compared with other works for stars in the thin disc (Adibekyan et al.

2012; Nissen et al. 2000; Reddy, Lambert & Allende Prieto 2006; Feltzing, Fohlman & Bensby 2007; Gilli et al. 2006; Takeda 2007), in the thick disc (Adibekyan et al. 2012; Nissen & Schuster 2011; Reddy, Lambert & Allende Prieto 2006; Feltzing, Fohlman & Bensby 2007; Ishigaki, Aoki & Chiba 2013), in the Galactic halo (Cayrel et al. 2004; Ishigaki, Aoki & Chiba 2013; Preston & Sneden 2000; Cohen et al. 2013; Hollek et al. 2011; Yong et al. 2013) and for different populations (Sobeck et al. 2006). Part of the observational scatter is due to the use of different Mn lines and different methods for the analysis in the papers presented above. Different works adopted the LTE approximation, while Bergemann & Gehren (2008) and Battistini & Bensby (2015) used the NLTE approach. As we have shown above, our measurements for [Mn/Fe] are only marginally affected by the LTE assumption. Therefore, we are confident that we can also compare our results with these works. Most of the authors observe a similar increasing [Mn/Fe] trends with the increasing of the metallicity in the Galactic disc for $-1 \lesssim [\text{Fe}/\text{H}] \lesssim 0.3$. Takeda (2007) did not observe any clear trend, but they used only one Mn line (5040 Å). Stars from Gilli et al. (2006) show a larger scatter at near-to-solar metallicity compared to other works: in particular, they obtain that stars hosting planetary systems show on average a larger Mn enrichment compared to stars without known planets.

The Mn abundances obtained for the thick and thin disc stellar populations in with no difference between the thin disc and the thick disc within uncertainties. Stars in our sample belonging to the Hercules Stream show abundances consistent with the other Galactic disc populations. A detailed comparison between our results and the literature is given in Tables 3, and 4. In particular, for stars in common with Feltzing, Fohlman & Bensby (2007) we obtain similar

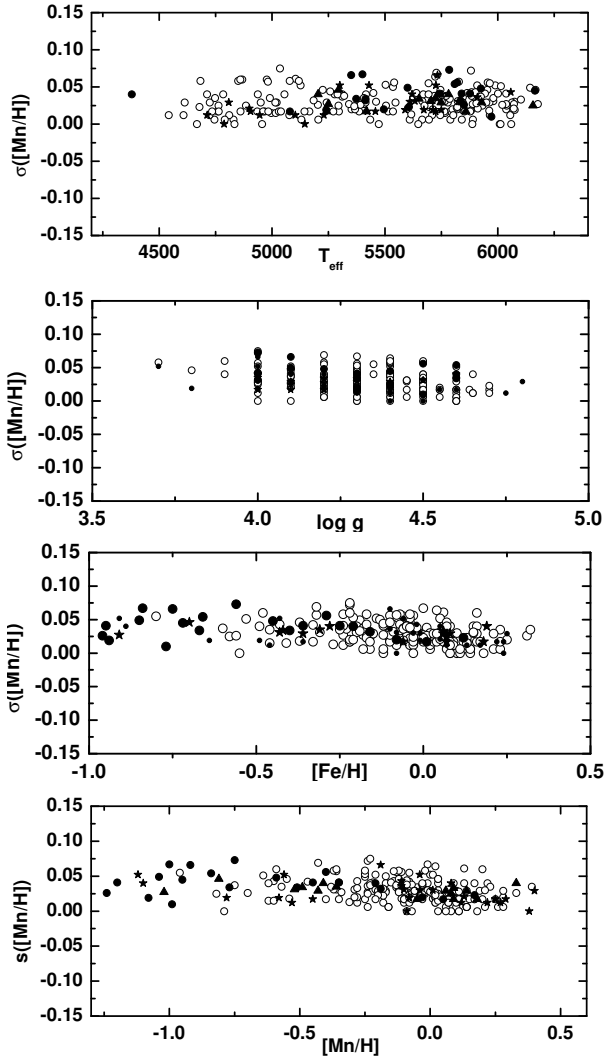


Figure 2. Dependences of σ [Mn/H] on atmospheric parameters, [Fe/H] and [Mn/H].

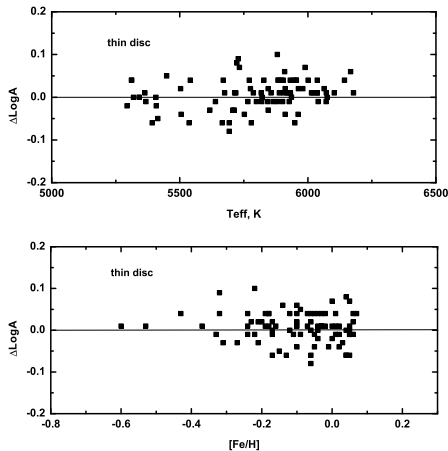


Figure 3. The dependence of the difference between Mn abundances determined with the Mn I lines at 4783 and 6013 AA for thin disc stars.

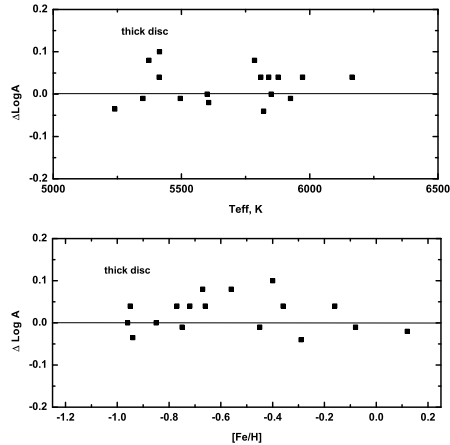


Figure 4. The dependence of the difference between Mn abundances determined with the Mn I lines at 4783 and 6013 AA for thick disc stars.

results. The only exception is HD199960, where we obtain a [Mn/Fe] lower by 0.21 dex that is within the errors of the two works. Note that the difference in the [Mn/Fe] for this star of our determination and the work of Battistini & Bensby (2015) is 0.06 dex. For other stars with Mn included in our sample and also measured by Battistini & Bensby (2015), the difference in [Mn/Fe] is within the determination error (0.10 dex) but for one star, HD 30495. In this case the difference is 0.15 dex, that is still consistent with our results within the errors given in BB 2015.

5 MN OBSERVATIONS AND DISCUSSION: IMPLICATIONS FROM THE NUCLEOSYNTHESIS OF MN IN STARS

In Fig. 6 we have shown the evolution of Mn compared to Fe for stars at different metallicities, ranging from low-metallicity stars to super-solar metallicities. For stars with [Fe/H] $\lesssim -1$, the abundance signature of Mn and Fe and therefore the observed [Mn/Fe] ratio is dominated by CC-SNe (e.g., Kobayashi, Karakas & Umeda 2011), while for higher metallicities the influence of SNe type Ia dominates. The only stable isotope of Mn (^{55}Mn) is made in explosive (complete and incomplete) Si-burning conditions as unstable ^{55}Co , which decays afterwards via ^{55}Fe to ^{55}Mn . In complete Si-burning this production occurs under normal freeze-out conditions only for sufficiently high densities and/or low entropies (see e.g., Thielemann, Nomoto & Yokoi 1986; Thielemann, Hashimoto & Nomoto 1990).

Such conditions exist only in (near-)Chandrasekhar mass SNe type Ia (Thielemann, Nomoto & Yokoi 1986; Iwamoto et al. 1999; Brachwitz et al. 2000; Seitzzahl et al. 2009, 2013b; Fink et al. 2014). In the α -rich regime of complete Si-burning (the only type of complete Si-burning experienced in CCSNe) ^{55}Co abundance is moved over to ^{59}Cu which decays via ^{59}Ni to ^{59}Co . However, ^{55}Co is also produced in incomplete Si-burning, which takes place in CCSNe as well as SNe Ia (Thielemann, Nomoto & Yokoi 1986; Woosley & Weaver 1995; Thielemann, Nomoto & Hashimoto 1996; Iwamoto et al. 1999; Nakamura et al. 1999; Brachwitz et al.

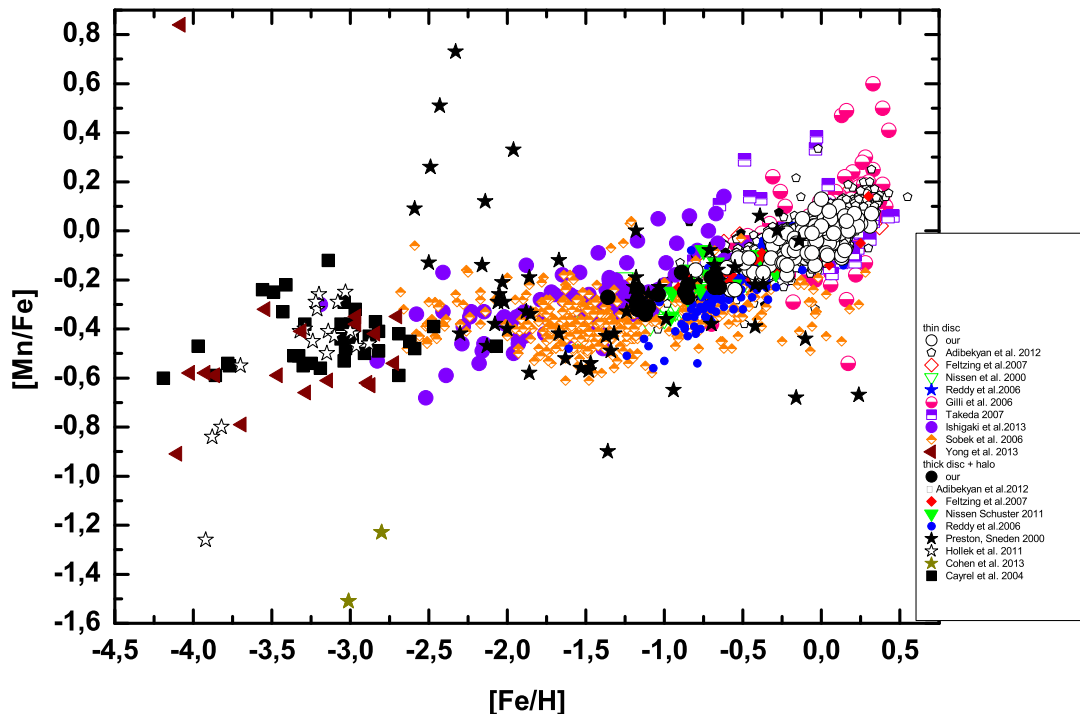


Figure 6. The trend of $[Mn/Fe]$ ratio with respect to $[Fe/H]$ is shown for our stellar sample, in comparison with the data of different authors. Markers are specified in the figure.

2000; Woosley, Heger & Weaver 2002). In all of these conditions, the production of ^{55}Co depends also on the electron fraction (Y_e) of the matter experiencing explosive burning. Y_e is the number of electrons per all nucleons (free and bound in nuclei), or the ratio of the number of all protons over all nucleons (i.e. neutrons plus protons). Thus, $Y_e = 0.5$ indicates a stellar composition with equal numbers of neutrons and protons, $Y_e < 0.5$ means that it is neutron-rich and $Y_e > 0.5$ that is proton-rich. In stellar evolution, the electron fraction Y_e first changes during H- and He-burning. Only marginal variations occur during the following C burning and Ne burning evolutionary stages. In advanced O-burning and then in Si-burning stages the Y_e decreases significantly (e.g., Thielemann & Arnett 1985). However, according to present theoretical stellar models these last regions will not be ejected by the SN explosion, or will not host the thermodynamic conditions needed to make Mn during the explosion.

There exists, however, a Y_e change in stellar models as a function of metallicity. In H-burning, the CNO-isotopes are burned essentially to ^{14}N (an $N=Z$ nucleus) which is moved in He-burning to ^{22}Ne (an $N=Z+2$ nucleus due to the beta-decay of ^{18}F to ^{18}O during the α -capture chain based on ^{14}N). In this way the metallicity (given predominantly by CNO abundances) is turned into the abundance of ^{22}Ne , which differs from the $Z/A=0.5$ of the other He-burning products and determines the electron fractions $Y_e = \sum_i Z_i Y_i$. For lowest metallicities ($[Fe/H]=-\infty$) this

relates to $Y_e = 0.5$ after He-burning, for solar metallicities ($[Fe/H]=0$) to $Y_e = 0.499$, for supersolar metallicities ($[Fe/H]=0.25, 0.5$) to $Y_e = 0.498, 0.496$. ^{55}Co , the radioactive progenitor of ^{55}Mn , has a $Z/A = 27/55$ of 0.491, which would be the Y_e -value at which the highest ^{55}Mn production is expected, while low metallicity stars would not produce ^{55}Mn if the Y_e is only determined by initial metallicity.

5.1 Massive stars

In massive stars, as we mentioned above, Mn is made mostly by the SN explosion in incomplete explosive Si-burning conditions as ^{55}Co (e.g., Woosley & Weaver 1995; Thielemann, Nomoto & Hashimoto 1996; Nakamura et al. 1999; Woosley, Heger & Weaver 2002). Mn production is increasing with the increase of the initial metallicity or, in other words, with the decrease of the electron fractions Y_e (e.g., Thielemann, Nomoto & Hashimoto 1996; Nakamura et al. 1999; Nomoto, Kobayashi & Tominaga 2013). Most of Fe is made as radiogenic ^{56}Fe from radioactive ^{56}Ni . This isotope is mainly made in complete explosive Si-burning conditions as primary product (i.e., independent of the initial metallicity of the star). However, a significant fraction is produced together with ^{55}Co in less extreme (incomplete Si-burning) SN conditions, but with an increasing production with increasing Y_e (or decreasing of the initial metallicity), which is the opposite compared to ^{55}Co . This scenario is becoming more complicated

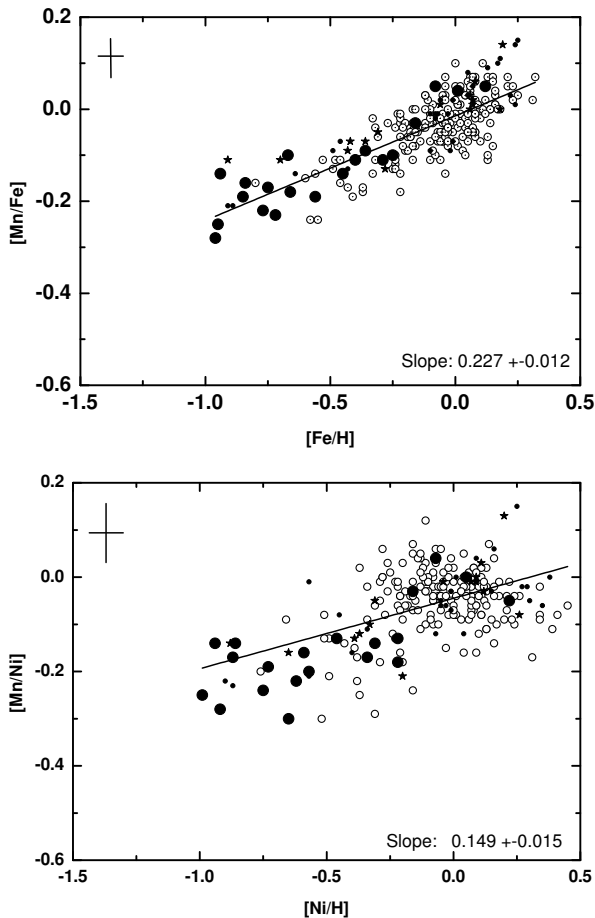


Figure 5. The trend of $[\text{Mn}/\text{Fe}]$ ratio with respect to $[\text{Fe}/\text{H}]$ is shown for our stellar sample: thin disc stars are marked as open symbols, thick disc stars as full symbols. Our determination for Hercules stream stars and unclassified stars are marked as black asterisks and points respectively. In the bottom figure we show the trend of $[\text{Mn}/\text{Ni}]$ ratio with respect to $[\text{Ni}/\text{H}]$.

once the zoo of different CCSN types is considered. For instance, Hypernovae tend to produce lower $[\text{Mn}/\text{Fe}]$ ratios compared to the less energetic SN Type-II, due to a larger production of ^{56}Ni and more extended α -rich freeze-out zones of complete Si-burning in comparison to incomplete Si-burning (e.g., Nakamura et al. 1999, 2001; Maeda et al. 2002). Asymmetries before and after the CCSN, and the SN-shock propagation through the massive star progenitor (e.g., Thielemann et al. 2011; Hix et al. 2014; Wongwathanarat, Mueller & Janka 2014) will affect the final Mn/Fe ratio in the SN ejecta, possibly explaining the large $[\text{Mn}/\text{Fe}]$ spread observed in the early Galaxy (Figure 6). Within this observational scatter, most of halo stars show an $[\text{Mn}/\text{Fe}] \sim -0.4$. Considering that CCSNe are producing about 30-50% of the Fe observed in the Solar system, this means that 12-20% of the solar Mn is made by CCSNe.

5.2 Type Ia supernovae

For $[\text{Fe}/\text{H}] \gtrsim -1$, the $[\text{Mn}/\text{Fe}]$ ratio in disc stars is increasing up to the solar ratio, due to the contribu-

tion from SNe Ia (SNIa, e.g., Hillebrandt et al. 2013) with on average $[\text{Mn}/\text{Fe}] > 0$. This is due to the fact that (near-)Chandrasekhar mass SNe type Ia experience also normal freeze-out conditions from nuclear statistical equilibrium in complete, explosive Si-burning, caused by high central densities and low entropies (see e.g., Thielemann, Nomoto & Yokoi 1986; Iwamoto et al. 1999; Brachwitz et al. 2000; Seitenzahl et al. 2009, 2013b; Fink et al. 2014). In these inner high-density regions, the Y_e is not due to the initial stellar metallicity (see introduction to this section), but caused by the capture of degenerate electrons with high Fermi energies on protons. Even the reduction of theoretical electron-capture rates (Brachwitz et al. 2000) did not change the amount of ^{55}Co produced in these inner zones, because a region of similar mass content with the relevant Y_e results also in that case. In particular, Yamaguchi et al. (2015) recently have reported the first direct observation of high Mn/Fe ratios in the SNIa remnant 3C 397, that can be explained only by the low Y_e due to electron captures. This makes 3C 397 an ideal candidate of a Chandrasekhar mass SNIa. In addition to these inner zones with normal freeze-out from complete Si-burning, also incomplete Si-burning is taking place in layers further out, where Y_e is determined by the initial metallicity, i.e. where the production of Mn and Fe depends on the initial composition of the stellar progenitor. This results in a situation where the production of Mn and Fe in the inner zones is independent on the initial metallicity (just due to electron capture as a function of central density), while the production of Mn and Fe in the outer zones depends on the initial metallicity (e.g., Nomoto, Thielemann & Yokoi 1984; Thielemann, Nomoto & Yokoi 1986; Iwamoto et al. 1999; Brachwitz et al. 2000; Thielemann et al. 2003; Seitenzahl et al. 2009, 2013b; Fink et al. 2014). If we take e.g. the results of (Iwamoto et al. 1999) for the (near-)Chandrasekhar mass type Ia explosion model W7 based on progenitor stars of zero and solar metallicity ($[\text{Fe}/\text{H}] = -\infty, 0$), this leads to composition ratios in the ejecta of $[\text{Mn}/\text{Fe}] = 0.067$ and 0.227 , which would of course find their way into the ISM and new stars only after the appropriate delay times for their formation with that initial metallicity. By scaling the Mn production in outer layers varying linearly with metallicity (but keeping constant the Mn yields from the inner ejecta dominated by electron-capture) this would lead for $[\text{Fe}/\text{H}] = 0.25$ and 0.5 to $[\text{Mn}/\text{Fe}] = 0.30$ and 0.38 , respectively. Other delayed detonation models find for solar metallicities values $[\text{Mn}/\text{Fe}] = 0.42$ (see Seitenzahl et al. 2013a). All (near-)Chandrasekhar mass models lead to $[\text{Mn}/\text{Fe}] > 0$, a contribution needed to explain the change from about -0.4 at low metallicities to $[\text{Mn}/\text{Fe}] > 0.3$ at supersolar metallicities.

Sub-Chandrasekhar mass type Ia models (see below) lack the inner electron-capture dominated Mn ejecta and contain only the outer metallicity dependent, incomplete Si-burning ejecta. Therefore, they will eject material with $[\text{Mn}/\text{Fe}] < 0$. The reproduction of the observed $[\text{Mn}/\text{Fe}]$ trend with respect to $[\text{Fe}/\text{H}]$ in the Galactic disc is an important diagnostic for Galactic chemical evolution and the (type Ia) supernova models contributing to it. The increasing $[\text{Mn}/\text{Fe}]$ trend has been considered as a signature: 1) of the gradual enrichment by SNIa ejecta of the ISM (Kobayashi & Nomoto 2009); 2) of the increasing

Mn/Fe ratio in the SNIa yields with the metallicity of the progenitor (Cescutti et al. 2008); 3) of the overlapping contribution of sub-Chandrasekhar SNe Ia made by WD mergers (e.g., Pakmor et al. 2010) or triggered by He-detonation on a single WD (e.g., Fink et al. 2010), and SNe Ia reaching the Chandrasekhar mass by accretion on a WD (e.g., Thielemann, Nomoto & Yokoi 1986; Iwamoto et al. 1999; Brachwitz et al. 2000; Thielemann et al. 2003; Seitzzahl et al. 2009, 2013b; Fink et al. 2014). This last result has been discussed recently by Seitzzahl et al. (2013a): sub-Chandrasekhar SNe Ia do not reach the conditions to make ^{55}Co in nuclear statistical equilibrium opposite to more massive SNe Ia, yielding low Mn/Fe ratio ejecta. Therefore, the [Mn/Fe] trend observed in the galactic disc may be used as an indirect diagnostic of the relative contribution from different types of SNe Ia. All the three arguments discussed above may play a role in defining the galactic trend of the [Mn/Fe] ratio, affecting in a similar way the evolution of the [Mn/Fe] with respect to [Fe/H]. The uncertainties associated with the nucleosynthesis of Mn and Fe in SNe Ia need to be also considered. While the nuclear uncertainties seem to be less relevant for this case (Parikh et al. 2013), other uncertainties associated with the SNIa explosion and to the stellar progenitor structure need to be considered.

Mn and Fe have an opposite dependence on the metallicity of the SNIa progenitor, which makes the analysis more complicated. The contribution to the solar inventory by CCSNe and SNe Ia is quite similar for Ni and Fe, yielding a quite flat [Ni/Fe] for stars with metallicities lower than solar in the disc and in the galactic halo (e.g., Kobayashi, Karakas & Umeda 2011; Mishenina et al. 2013, and references therein). As discussed in Mishenina et al. (2013), Ni is a primary product both in CCSNe and in SNe Ia, made by nuclear statistical equilibrium in both the two stellar sources (see Jerkstrand et al. 2015, for a recent analysis of Ni production compared to Fe in CCSN conditions). Therefore, for basic nucleosynthesis reasons the evolution of the [Mn/Ni] ratio should be an observational diagnostic for the production of Mn in stars much easier to study than the [Mn/Fe] ratio.

We need to remind that the reproduction of the observed [Ni/Fe] trend in the galaxy has been proven to be challenging for GCE simulations, both in the halo and in the galactic disc (e.g., Goswami & Prantzos 2000; Kobayashi, Karakas & Umeda 2011). While assumptions made by GCE models may be an important source of uncertainty, the present issues to reproduce the [Ni/Fe] galactic trend is related to the present limitations in theoretical stellar models and, as a consequence, in the stellar yields used by GCE simulations. On the other hand, a confirmation of theoretical results comes for SNe Ia with close-to Chandrasekhar mass, with these objects yielding high Ni/Fe and low Mn/Ni ejecta (Yamaguchi et al. 2015). This means that the [Mn/Ni] ratio can be also used to distinguish different SNIa populations together with the [Mn/Fe] ratio, but without being affected by the metallicity dependence associated with the Fe yields of SNe Ia. Consistent observations for Mn, Fe and Ni on the same stellar samples are important to study the production of Fe-group elements in SNe Ia. GCE studies aiming to deliver robust conclusions about

the nucleosynthesis of Mn, should take into account both Fe and Ni as reference elements.

In order to study the impact of this in our analysis, we also compare the Mn abundance with Ni (Fig. 5). The average error for [Mn/Ni] is about 0.15 dex (Mishenina et al. 2013). For our stellar sample, the average observed slope for [Mn/Fe] with respect to [Fe/H] is 0.227 ± 0.012 , while we obtain for [Mn/Ni] with respect to [Ni/H] 0.149 ± 0.015 . The two slopes are different. For the considerations made before, we may expect to observe a steeper slope for [Mn/Fe] compared to [Mn/Ni]. This confirms that the metallicity dependence of Fe yields in SNe Ia may play a role in the [Mn/Fe] and [Ni/Fe] trends. The impact of this with respect to the contribution from different SNIa populations to Mn, Fe and Ni still has to be investigated. At the moment we cannot derive any quantitative conclusion, since our thick disc sample does not include enough stars and because of observational errors. Furthermore, in our stellar sample we observe a larger dispersion of the [Mn/Ni] data compared to [Mn/Fe] in Fig. 5, in particular for thin disc stars.

6 CONCLUSIONS AND FINAL REMARKS.

In this work we presented and discussed the abundance measurements of Mn for 247 disc stars. The analysis is based on LTE assumptions. The insufficient accuracy of atomic data makes difficult to construct an adequate model for NLTE calculations for Mn. We show that in our case the corrections by Bergemann & Gehren (2008) are not confirmed by observations. We have discussed the uncertainties affecting the determination of the Mn abundance. For [Mn/Fe] we obtain an error of about 0.10 dex. The major source of its uncertainty is the choice of the temperature.

For disc stars in our stellar sample we obtain an increasing [Mn/Fe] trend with [Fe/H] consistent with most of other works. Within observational uncertainties we cannot disentangle the abundance patterns for thin disc and thick disc stars, as obtained by Feltzing, Fohlman & Bensby (2007); Battistini & Bensby (2015). On the other hand, our determinations of [Mn/Fe] are consistent with the data of these two works for common stars within the observational errors. We have compared the [Mn/Fe] and [Mn/Ni] trends with [Fe/H] and [Ni/H], respectively. The reason is that Mn and Fe production in SNe Ia both depend on the initial metallicity of the progenitor with opposite trends: Mn yields increase with the metallicity of the SNIa progenitor, while Fe yields decrease. On the other hand, Ni production is independent from the initial stellar metallicity. We show that the [Mn/Ni] and [Mn/Fe] patterns have an average slope of 0.149 ± 0.015 and 0.227 ± 0.012 , respectively. While the slopes are different within 2σ , the [Mn/Ni] observational dispersion for thin disc stars and our small sample of thick disc stars do not allow to derive quantitative conclusions.

We reviewed the production of Mn and Fe in SNe Ia and CCSNe. In particular, there are three main scenarios that are qualitatively compatible with the observed [Mn/Fe] pattern in the galactic disc, including the relative contribution from both sub-Chandrasekhar mass SNe Ia and more massive SNe Ia. In order to define the relative frequency of the different SNIa populations explaining the [Mn/Fe] observations, the impact of the other two aspects need to be

disentangled and weighted consistently by a detailed GCE study.

ACKNOWLEDGEMENTS

TM, TG, MP, FKT and SK thank for the support from the Swiss National Science Foundation, project SCOPES No. IZ73Z0152485. MP acknowledges significant support to NuGrid from NSF grants PHY 09-22648 (Joint Institute for Nuclear Astrophysics, JINA), NSF grant PHY-1430152 (JINA Center for the Evolution of the Elements) and EU MIRG-CT-2006-046520. MP acknowledges the support from the "Lendlet-2014" Programme of the Hungarian Academy of Sciences (Hungary) and from SNF (Switzerland). FKT acknowledges support from the European Research Council (FP7) under ERC Advanced Grant Agreement 321263 FISH.

REFERENCES

- Adibekyan V. Z., Sousa S. G., Santos N. C., Delgado Mena E., González Hernández J. I., Israelian G., Mayor M., Khachatryan G., 2012, *A&A*, 545, A32
- Allende Prieto C., García López R. J., Lambert D. L., Gustafsson B., 1999, *ApJ*, 527, 879
- Alves-Brito A., Barbuy B., Allen D. M., 2007, in *IAU Symposium*, Vol. 241, *IAU Symposium*, Vazdekis A., Peletier R., eds., pp. 231–232
- Andrievsky S. M., Korotin S. A., Martin P., 2007, *A&A*, 464, 709
- Baranne A. et al., 1996, *A&AS*, 119, 373
- Battistini C., Bensby T., 2015, *A&A*, 577, A9
- Bergemann M., Gehren T., 2007, *A&A*, 473, 291
- Bergemann M., Gehren T., 2008, *A&A*, 492, 823
- Brachwitz F. et al., 2000, *ApJ*, 536, 934
- Bravo E., Domínguez I., Badenes C., Piersanti L., Straniero O., 2010, *ApJ*, 711, L66
- Castelli F., Kurucz R. L., 2004, *ArXiv Astrophysics e-prints*
- Cayrel R. et al., 2004, *A&A*, 416, 1117
- Cescutti G., Matteucci F., Lanfranchi G. A., McWilliam A., 2008, *A&A*, 491, 401
- Cohen J. G., Christlieb N., Thompson I., McWilliam A., Shectman S., Reimers D., Wisotzki L., Kirby E., 2013, *ApJ*, 778, 56
- Cunha K., Smith V. V., Bergemann M., Suntzeff N. B., Lambert D. L., 2010, *ApJ*, 717, 333
- Feltzing S., Fohlman M., Bensby T., 2007, *A&A*, 467, 665
- Fink M. et al., 2014, *MNRAS*, 438, 1762
- Fink M., Röpké F. K., Hillebrandt W., Seitzzahl I. R., Sim S. A., Kromer M., 2010, *A&A*, 514, A53
- Fröhlich C. et al., 2006, *ApJ*, 637, 415
- Galazutdinov G. A., 1992, *Preprint SAO RAS*
- Gilli G., Israelian G., Ecuivillon A., Santos N. C., Mayor M., 2006, *A&A*, 449, 723
- Goswami A., Prantzos N., 2000, *A&A*, 359, 191
- Gratton R. G., 1989, *A&A*, 208, 171
- Hawkins K., Jofre P., Masseron T., Gilmore G., 2015, *ArXiv e-prints*
- Hillebrandt W., Kromer M., Röpké F. K., Ruiter A. J., 2013, *Frontiers of Physics*, 8, 116
- Hix W. R. et al., 2014, *AIP Advances*, 4, 041013
- Hollek J. K., Frebel A., Roederer I. U., Sneden C., Shetrone M., Beers T. C., Kang S.-j., Thom C., 2011, *ApJ*, 742, 54
- Ishigaki M. N., Aoki W., Chiba M., 2013, *ApJ*, 771, 67
- Iwamoto K., Brachwitz F., Nomoto K., Kishimoto N., Umeda H., Hix W. R., Thielemann F.-K., 1999, *ApJS*, 125, 439
- Jerkstrand A. et al., 2015, *ApJ*, 807, 110
- Katz D., Soubiran C., Cayrel R., Adda M., Cautain R., 1998, *A&A*, 338, 151
- Kobayashi C., Karakas A. I., Umeda H., 2011, *MNRAS*, 414, 3231
- Kobayashi C., Nomoto K., 2009, *ApJ*, 707, 1466
- Kovtyukh V. V., Soubiran C., Belik S. I., Gorlova N. I., 2003, *A&A*, 411, 559
- Kupka F., Piskunov N., Ryabchikova T. A., Stempels H. C., Weiss W. W., 1999, *A&AS*, 138, 119
- Limongi M., Straniero O., Chieffi A., 2000, *ApJS*, 129, 625
- Maeda K., Nakamura T., Nomoto K., Mazzali P. A., Patat F., Hachisu I., 2002, *ApJ*, 565, 405
- Matteucci F., Greggio L., 1986, *A&A*, 154, 279
- Matteucci F., Spitoni E., Recchi S., Valiante R., 2009, *A&A*, 501, 531
- McWilliam A., Rich R. M., Smecker-Hane T. A., 2003, *ApJ*, 592, L21
- Mishenina T. V., Kovtyukh V. V., 2001, *A&A*, 370, 951
- Mishenina T. V., Pignatari M., Korotin S. A., Soubiran C., Charbonnel C., Thielemann F.-K., Gorbaneva T. I., Basak N. Y., 2013, *A&A*, 552, A128
- Mishenina T. V., Soubiran C., Bienayme O., Korotin S. A., Belik S. I., Usenko I. A., Kovtyukh V. V., 2008, *A&A*, 489, 923
- Mishenina T. V., Soubiran C., Kovtyukh V. V., Korotin S. A., 2004, *A&A*, 418, 551
- Nakamura T., Umeda H., Iwamoto K., Nomoto K., Hashimoto M.-a., Hix W. R., Thielemann F.-K., 2001, *ApJ*, 555, 880
- Nakamura T., Umeda H., Nomoto K., Thielemann F.-K., Burrows A., 1999, *ApJ*, 517, 193
- Nissen P. E., Chen Y. Q., Schuster W. J., Zhao G., 2000, *A&A*, 353, 722
- Nissen P. E., Schuster W. J., 2011, *A&A*, 530, A15
- Nomoto K., Kobayashi C., Tominaga N., 2013, *ARA&A*, 51, 457
- Nomoto K., Thielemann F.-K., Yokoi K., 1984, *ApJ*, 286, 644
- Nomoto K., Tominaga N., Umeda H., Kobayashi C., Maeda K., 2006, *Nuclear Physics A*, 777, 424
- Pakmor R., Kromer M., Röpké F. K., Sim S. A., Ruiter A. J., Hillebrandt W., 2010, *Nature*, 463, 61
- Pancino E., Mucciarelli A., Sbordone L., Bellazzini M., Pasquini L., Monaco L., Ferraro F. R., 2011, *A&A*, 527, A18
- Parikh A., José J., Seitzzahl I. R., Röpké F. K., 2013, *A&A*, 557, A3
- Perruchot S. et al., 2008, in *Society of Photo-Optical Instrumentation Engineers (SPIE) Conference Series*, Vol. 7014, *Society of Photo-Optical Instrumentation Engineers (SPIE) Conference Series*, p. 12
- Preston G. W., Sneden C., 2000, *AJ*, 120, 1014

- Prochaska J. X., Naumov S. O., Carney B. W., McWilliam A., Wolfe A. M., 2000, *AJ*, 120, 2513
- Reddy B. E., Lambert D. L., Allende Prieto C., 2006, *MNRAS*, 367, 1329
- Seitenzahl I. R., Cescutti G., Röpke F. K., Ruiter A. J., Pakmor R., 2013a, *A&A*, 559, L5
- Seitenzahl I. R. et al., 2013b, *MNRAS*, 429, 1156
- Seitenzahl I. R., Meakin C. A., Lamb D. Q., Truran J. W., 2009, *ApJ*, 700, 642
- Sobeck J. S., Ivans I. I., Simmerer J. A., Sneden C., Hoefflich P., Fulbright J. P., Kraft R. P., 2006, *AJ*, 131, 2949
- Takeda Y., 2007, *PASJ*, 59, 335
- Thielemann F.-K. et al., 2003, in *From Twilight to High-light: The Physics of Supernovae*, Hillebrandt W., Leibundgut B., eds., p. 331
- Thielemann F. K., Arnett W. D., 1985, *ApJ*, 295, 604
- Thielemann F.-K., Hashimoto M.-A., Nomoto K., 1990, *ApJ*, 349, 222
- Thielemann F.-K., Hirschi R., Liebendörfer M., Diehl R., 2011, in *Lecture Notes in Physics*, Berlin Springer Verlag, Vol. 812, *Lecture Notes in Physics*, Berlin Springer Verlag, Diehl R., Hartmann D. H., Prantzos N., eds., pp. 153–232
- Thielemann F.-K., Nomoto K., Hashimoto M.-A., 1996, *ApJ*, 460, 408
- Thielemann F.-K., Nomoto K., Yokoi K., 1986, *A&A*, 158, 17
- Timmes F. X., Brown E. F., Truran J. W., 2003, *ApJ*, 590, L83
- Timmes F. X., Woosley S. E., Weaver T. A., 1995, *ApJS*, 98, 617
- Travaglio C., Hillebrandt W., Reinecke M., 2005, *A&A*, 443, 1007
- Tsymbal V., 1996, in *Astronomical Society of the Pacific Conference Series*, Vol. 108, M.A.S.S., *Model Atmospheres and Spectrum Synthesis*, Adelman S. J., Kupka F., Weiss W. W., eds., p. 198
- Umeda H., Nomoto K., 2005, *ApJ*, 619, 427
- Wallerstein G., 1962, *ApJS*, 6, 407
- Wongwathanarat A., Mueller E., Janka H.-T., 2014, *ArXiv e-prints*
- Woosley S. E., Heger A., Weaver T. A., 2002, *Reviews of Modern Physics*, 74, 1015
- Woosley S. E., Weaver T. A., 1995, *ApJS*, 101, 181
- Yamaguchi H. et al., 2015, *ApJ*, 801, L31
- Yong D. et al., 2013, *ApJ*, 762, 26

Table 1: Atmospheric parameters and Mn abundance $\log A(\text{Mn})$ each used line (λ , A) and $[\text{Mn}/\text{Fe}]$ ratio for our target stars

Star	$T_{\text{eff},\text{K}}$	$\log g$	Vt	[Fe/H]	4783, A	4823,A	5432,A	6013,A	6021, A	[Mn/Fe]
Sun					5.3	5.25	5.27	5.24	5.24	
Thick disk										
HD245	5400	3.4	-0.84	0.7	4.32	4.35	4.1	4.18	4.18	-0.16
HD3765	5079	4.3	0.01	1.1			5.3	5.3	5.3	0.04
HD6582	5240	4.3	-0.94	0.7	4.2	4.2	4.18	4.15	4.15	-0.14
HD13783	5350	4.1	-0.75	1.1	4.35	4.4	4.4		4.25	-0.17
HD18757	5741	4.3	-0.25	1	4.95	4.95	4.95	4.85	4.85	-0.1
HD22879	5972	4.5	-0.77	1.1	4.31	4.28		4.25	4.25	-0.22
HD65583	5373	4.6	-0.67	0.7	4.5	4.5	4.55	4.45	4.45	-0.1
HD76932	5840	4	-0.95	1	4.05	4.1		4.05	4.05	-0.25
HD106516	6165	4.4	-0.72	1.1	4.35	4.35			4.25	-0.23
HD110897	5925	4.2	-0.45	1.1	4.7	4.7	4.73	4.6	4.6	-0.14
HD135204	5413	4	-0.16	1.1	5.15	5.05	5.08	5.05	5	-0.03
HD152391	5495	4.3	-0.08	1.3	5.25	5.25	5.25	5.2	5.2	0.05
HD157089	5785	4	-0.56	1	4.58	4.6	4.55	4.42	4.42	-0.19
HD157214	5820	4.5	-0.29	1	4.92	4.92	4.88	4.78	4.78	-0.11
HD159062	5414	4.3	-0.4	1	4.75	4.75	4.8	4.75	4.7	-0.11
HD165401	5877	4.3	-0.36	1.1	4.85	4.85	4.85	4.75	4.75	-0.09
HD190360	5606	4.4	0.12	1.1			5.47	5.4	5.4	0.05
HD201889	5600	4.1	-0.85	1.2	4.2	4.23	4.3	4.18	4.18	-0.19
HD201891	5850	4.4	-0.96	1	4.05	4.05		4	3.98	-0.28
HD204521	5809	4.6	-0.66	1.1	4.45	4.45	4.5	4.35	4.35	-0.18
Thin disk										
HD166	5514	4.6	0.16	0.6			5.42	5.42	5.42	0.01
HD1562	5828	4	-0.32	1.2	4.95	4.97		4.85	4.83	-0.04
HD1835	5790	4.5	0.13	1.1			5.45	5.45	5.45	0.07
HD3651	5277	4.5	0.15	0.6			5.45	5.45	5.5	0.07
HD4256	5020	4.3	0.08	1.1			5.38	5.4	5.4	0.06
HD4307	5889	4	-0.18	1.1	5.05	5.05	5.05	4.98	4.98	-0.06
HD4614	5965	4.4	-0.24	1.1			5	4.95	4.95	-0.04
HD5294	5779	4.1	-0.17	1.3	5.08	5.1	5.12	5.08	5.08	0
HD6660	4759	4.6	0.08	1.4			5.4	5.4	5.4	0.07
HD7590	5962	4.4	-0.1	1.4	5.17	5.15	5.15	5.15	5.15	-0.01
HD7924	5165	4.4	-0.22	1.1			5	5	5	-0.03
HD8648	5790	4.2	0.12	1.1			5.4	5.38	5.38	0.02
HD9407	5666	4.45	0.05	0.8	5.25	5.25	5.22	5.25	5.25	-0.07
HD9826	6074	4	0.1	1.3			5.27	5.3	5.27	-0.07
HD10086	5696	4.3	0.13	1.2			5.32	5.25	5.25	-0.11
HD10307	5881	4.3	0.02	1.1	5.3	5.28	5.28	5.25	5.22	-0.01
HD10476	5242	4.3	-0.05	1.1			5.2	5.12	5.12	-0.05
HD10780	5407	4.3	0.04	0.9	5.3	5.3	5.24	5.24	5.24	-0.04
HD11007	5980	4	-0.2	1.1	5	5	5	4.92	4.92	-0.09
HD11373	4783	4.65	0.08	1			5.35	5.25	5.25	-0.05
HD12846	5766	4.5	-0.24	1.2	4.92	4.92	4.94	4.87	4.84	-0.12
HD13507	5714	4.5	-0.02	1.1	5.22	5.22	5.26	5.15	5.18	-0.03
HD14374	5449	4.3	-0.09	1.1	5.24	5.24	5.18	5.13	5.13	0.01
HD16160	4829	4.6	-0.16	1.1			5.12	5.08	5.08	0
HD17674	5909	4	-0.14	1.1	5.12	5.12	5.05	5	4.98	-0.07
HD17925	5225	4.3	-0.04	1.1			5.25	5.3	5.3	0.07
HD18632	5104	4.4	0.06	1.4			5.33	5.38	5.42	0.07
HD18803	5665	4.55	0.14	0.8			5.4	5.38	5.38	0
HD19019	6063	4	-0.17	1.1	5.08	5.08	5.05	5	5	-0.05
HD19373	5963	4.2	0.06	1.1	5.4	5.4	5.36	5.32	5.32	0.04
HD20630	5709	4.5	0.08	1.1			5.3	5.25	5.25	-0.06
HD22484	6037	4.1	-0.03	1.1	5.22	5.2	5.22	5.15	5.15	-0.04
HD24053	5723	4.4	0.04	1.1	5.35	5.35		5.21	5.21	-0.02
HD24238	4996	4.3	-0.46	1			4.65	4.63	4.6	-0.16

Table 1: Continued.

Star	$T_{\text{eff},\text{K}}$	$\log g$	Vt	[Fe/H]	4783, A	4823,A	5432,A	6013,A	6021, A	[Mn/Fe]
HD24496	5536	4.3	-0.13	1.5	5.08	5.08	5.18	5.08	5.04	-0.04
HD25665	4967	4.7	0.01	1.2			5.18	5.18	5.18	-0.08
HD25680	5843	4.5	0.05	1.1	5.3	5.3	5.28	5.25	5.25	-0.03
HD26923	5920	4.4	-0.03	1	5.2	5.2	5.12	5.13	5.13	-0.07
HD28447	5639	4	-0.09	1.1	5.15	5.15	5.22	5.1	5.1	-0.03
HD29150	5733	4.3	0	1.1	5.31	5.33		5.18	5.18	-0.01
HD29310	5852	4.2	0.08	1.4			5.32	5.32	5.32	-0.01
HD29645	6009	4	0.14	1.3			5.38	5.35	5.35	-0.03
HD30495	5820	4.4	-0.05	1.3	5.2	5.2	5.2	5.15	5.15	-0.03
HD33632	6072	4.3	-0.24	1.1	4.95	4.95	4.95	4.88	4.88	-0.1
HD34411	5890	4.2	0.1	1.1			5.36	5.34	5.34	0
HD37008	5016	4.4	-0.41	0.8			4.68	4.64	4.62	-0.19
HD37394	5296	4.5	0.09	1.1			5.35	5.35	5.35	0.01
HD38858	5776	4.3	-0.23	1.1	5.05	5.05	5.07	4.97	4.97	-0.01
HD39587	5955	4.3	-0.03	1.5	5.2	5.2	5.2	5.1	5.05	-0.08
HD40616	5881	4	-0.22	1.1	5.08	5.08	5.08	4.92	4.92	-0.02
HD41330	5904	4.1	-0.18	1.2	5.08	5.08	5.08	4.98	4.98	-0.04
HD41593	5312	4.3	-0.04	1.1	5.3	5.3	5.23	5.2	5.2	0.03
HD42618	5787	4.5	-0.07	1	5.15	5.15	5.18	5.08	5.08	-0.06
HD42807	5719	4.4	-0.03	1.1	5.22	5.25	5.2	5.15	5.15	-0.04
HD43587	5927	4.1	-0.11	1.3	5.2	5.2	5.2	5.15	5.12	0.02
HD43856	6143	4.1	-0.19	1.1	5.05	5.08	5.02	4.95	4.95	-0.06
HD43947	6001	4.3	-0.24	1.1	4.95	4.95	4.95	4.85	4.85	-0.11
HD47752	4613	4.6	-0.05	0.2			5.18	5.1	5.1	-0.07
HD48682	5989	4.1	0.05	1.3	5.33	5.33	5.25	5.2	5.2	-0.05
HD50281	4712	3.9	-0.2	1.6			5	5	5.05	-0.03
HD50692	5911	4.5	-0.1	0.9	5.08	5.08	5.08	5	5	-0.11
HD51419	5746	4.1	-0.37	1.1		4.75		4.68	4.65	-0.18
HD51866	4934	4.4	0	1			5.3	5.3	5.3	0.05
HD53927	4860	4.64	-0.22	1.2			4.85	4.85	4.85	-0.18
HD54371	5670	4.2	0.06	1.2	5.4	5.4	5.33	5.3	5.3	0.03
HD58595	5707	4.3	-0.31	1.2	4.9	4.92		4.87	4.85	-0.06
HD59747	5126	4.4	-0.04	1.1			5.22	5.28	5.28	0.05
HD61606	4956	4.4	-0.12	1.3			5.18	5.15	5.15	0.03
HD62613	5541	4.4	-0.1	1.1	5.17	5.2	5.17	5.07	5.05	-0.03
HD63433	5693	4.35	-0.06	1.9	5.08	5.08	5.15	5.1	5.05	-0.11
HD63433	5693	4.35	-0.06	1.5	5.15	5.25	5.2	5.15	5.13	-0.02
HD64468	5014	4.2	0	1.2			5.4	5.32	5.32	0.1
HD64815	5864	4	-0.33	1.1	4.8	4.83	4.83	4.75	4.72	-0.14
HD65874	5936	4	0.05	1.3	5.4	5.4	5.4	5.34	5.32	0.06
HD72905	5884	4.4	-0.07	1.5	5.17	5.17		5.07	5.07	-0.07
HD73344	6060	4.1	0.08	1.1				5.27	5.27	-0.05
HD73667	4884	4.4	-0.58	0.9			4.45	4.45	4.4	-0.24
HD91347	5931	4.4	-0.43	1.1	4.71	4.71		4.61	4.61	-0.17
HD101177	5932	4.1	-0.16	1.1	5.05	5.05	5.02	4.98	4.98	-0.08
HD102870	6055	4	0.13	1.4			5.35	5.3	5.3	-0.06
HD105631	5416	4.4	0.16	1.2			5.4	5.4	5.45	0.01
HD107705	6040	4.2	0.06	1.4	5.3	5.3	5.25	5.25	5.25	-0.05
HD108954	6037	4.4	-0.12	1.1	5.15	5.15	5.15	5.05	5.05	-0.03
HD109358	5897	4.2	-0.18	1.1	5.08	5.08	5.05	4.98	4.98	-0.05
HD110463	4950	4.5	-0.05	1.2			5.2	5.12	5.12	-0.05
HD111395	5648	4.6	0.1	0.9			5.35	5.32	5.32	-0.02
HD112758	5203	4.2	-0.56	1.1			4.56	4.57	4.52	-0.14
HD114710	5954	4.3	0.07	1.1	5.35	5.35	5.25	5.25	5.25	-0.04
HD115383	6012	4.3	0.11	1.1			5.38	5.35	5.35	0
HD115675	4745	4.45	0.02	1			5.32	5.3	5.3	0.04
HD116443	4976	3.9	-0.48	1.1			4.6	4.65	4.73	-0.11
HD116956	5386	4.55	0.08	1.2			5.35	5.35	5.35	0.02
HD117043	5610	4.5	0.21	0.4			5.52	5.5	5.5	0.05

Table 1: Continued.

Star	$T_{\text{eff,K}}$	$\log g$	Vt	[Fe/H]	4783, A	4823,A	5432,A	6013,A	6021, A	[Mn/Fe]
HD119802	4763	4	-0.05	1.1			5.25	5.2	5.25	0.03
HD122064	4937	4.5	0.07	1.1			5.45	5.35	5.35	0.06
HD124642	4722	4.65	0.02	1.3			5.35	5.3	5.3	0.05
HD125184	5695	4.3	0.31	0.7			5.58	5.56	5.6	0.02
HD126053	5728	4.2	-0.32	1.1	4.9	4.9		4.75	4.75	-0.11
HD127506	4542	4.6	-0.08	1.2			5.1	5.05	5.05	-0.1
HD128311	4960	4.4	0.03	1.3			5.22	5.22	5.22	-0.06
HD130307	4990	4.3	-0.25	1.4			4.85	4.88	4.88	-0.13
HD130948	5943	4.4	-0.05	1.3	5.18	5.18	5.18	5.08	5.08	-0.07
HD131977	4683	3.7	-0.24	1.8			4.85	4.93	4.96	-0.13
HD135599	5257	4.3	-0.12	1			5.15	5.13	5.2	0.03
HD137107	6037	4.3	0	1.1	5.22	5.22	5.22	5.15	5.15	-0.07
HD139777	5771	4.4	0.01	0.7	5.28	5.28	5.22	5.18	5.18	-0.04
HD139813	5408	4.5	0	0.9	5.26	5.28	5.24	5.22	5.22	-0.02
HD140538	5675	4.5	0.02	0.9	5.32	5.32	5.3	5.25	5.25	0.01
HD141004	5884	4.1	-0.02	1.1	5.28	5.28	5.22	5.18	5.18	-0.01
HD141272	5311	4.4	-0.06	1.3	5.18	5.18	5.15	5.08	5.08	-0.07
HD142267	5856	4.5	-0.37	1.1	4.75	4.72	4.75	4.68	4.68	-0.17
HD144287	5414	4.5	-0.15	1.1	5.05	5.05	5.1	5.04	5.04	-0.05
HD145675	5406	4.5	0.32	1.3			5.7	5.63	5.6	0.07
HD146233	5799	4.4	0.01	1.1	5.3	5.3	5.3	5.25	5.25	0.01
HD149661	5294	4.5	-0.04	1.1	5.22	5.22	5.18	5.18	5.15	-0.03
HD149806	5352	4.55	0.25	0.4			5.53	5.52	5.54	0.03
HD151541	5368	4.2	-0.22	1.3	5	5	5	4.95	4.95	-0.06
HD153525	4810	4.7	-0.04	1.0			5.18	5.13	5.13	-0.06
HD154345	5503	4.3	-0.21	1.3	5.05	5.08		4.97	4.95	-0.04
HD156668	4850	4.2	-0.07	1.2			5.08	5.15	5.15	-0.05
HD156985	4790	4.6	-0.18	1.0			5.02	5	5	-0.06
HD158633	5290	4.2	-0.49	1.3			4.7	4.6	4.6	-0.13
HD160346	4983	4.3	-0.1	1.1			5.15	5.15	5.15	0
HD161098	5617	4.3	-0.27	1.1	4.98	4.95		4.95	4.93	-0.03
HD164922	5392	4.3	0.04	1.1	5.32	5.32	5.35	5.32	5.32	0.03
HD165173	5505	4.3	-0.05	1.1	5.2	5.22	5.22	5.18	5.18	-0.01
HD165476	5845	4.1	-0.06	1.1	5.18	5.18	5.2	5.1	5.1	-0.05
HD165670	6178	4	-0.1	1.5	5.12	5.12	5.12	5.05	5.05	-0.07
HD165908	5925	4.1	-0.6	1.1	4.55	4.55	4.4	4.48	4.45	-0.15
HD166620	5035	4	-0.22	1			4.95	5.05	5.05	-0.01
HD171314	4608	4.65	0.07	1.0			5.3	5.25	5.25	-0.05
HD174080	4764	4.55	0.04	1.0			5.32	5.32	5.32	0.03
HD175742	5030	4.5	-0.03	2.0			5.15	5.15	5.15	-0.07
HD176377	5901	4.4	-0.17	1.3	5	5	5.04	4.95	4.9	-0.11
HD176841	5841	4.3	0.23	1.1			5.56	5.52	5.52	0.05
HD178428	5695	4.4	0.14	1.1			5.42	5.38	5.38	0
HD180161	5473	4.5	0.18	1.1			5.45	5.42	5.42	0
HD182488	5435	4.4	0.07	1.1			5.42	5.38	5.38	0.07
HD183341	5911	4.3	-0.01	1.3	5.2	5.2	5.22	5.18	5.18	-0.05
HD184385	5536	4.45	0.12	0.9			5.36	5.36	5.36	-0.01
HD185144	5271	4.2	-0.33	1.1			4.9	4.9	4.9	-0.02
HD185414	5818	4.3	-0.04	1.1	5.13	5.1	5.08	5.06	5.03	-0.14
HD186408	5803	4.2	0.09	1.1			5.38	5.33	5.33	0.01
HD186427	5752	4.2	0.02	1.1	5.25	5.27	5.28	5.23	5.2	-0.03
HD187897	5887	4.3	0.08	1.1			5.33	5.3	5.3	-0.02
HD189087	5341	4.4	-0.12	1.1	5.16	5.16	5.18	5.1	5.1	0
HD189733	5076	4.4	-0.03	1.5			5.2	5.15	5.15	-0.05
HD190007	4724	4.5	0.16	0.8			5.43	5.45	5.45	0.03
HD190406	5905	4.3	0.05	1.1	5.3	5.3	5.25	5.23	5.23	-0.05
HD190470	5130	4.3	0.11	1			5.47	5.45	5.45	0.1
HD190771	5766	4.3	0.13	1.5			5.3	5.28	5.25	-0.1
HD191533	6167	3.8	-0.1	1.5	5.2	5.2	5.15	5.08	5.08	-0.02

Table 1: Continued.

Star	T_{eff} ,K	$\log g$	Vt	[Fe/H]	4783, A	4823,A	5432,A	6013,A	6021, A	[Mn/Fe]
HD191785	5205	4.2	-0.12	1.2			5.1	5.08	5.08	-0.04
HD195005	6075	4.2	-0.06	1.3	5.21	5.2	5.21	5.15	5.15	-0.02
HD195104	6103	4.3	-0.19	1.1	5.02	5.02	4.95	4.95	4.95	-0.09
HD197076	5821	4.3	-0.17	1.2	5.08	5.08	5.08	5.02	5.02	-0.03
HD199960	5878	4.2	0.23	1.1			5.5	5.5	5.5	0.02
HD200560	5039	4.4	0.06	1.1			5.36	5.36	5.36	0.05
HD202108	5712	4.2	-0.21	1.1	4.98	4.98	5	4.95	4.95	-0.08
HD202575	4667	4.6	-0.03	0.5			5.2	5.17	5.17	-0.04
HD203235	6071	4.1	0.05	1.3	5.33	5.33	5.3	5.28	5.28	-0.01
HD205702	6020	4.2	0.01	1.1	5.32	5.3	5.3	5.25	5.22	0.01
HD208038	4982	4.4	-0.08	1			5.07	5.12	5.15	-0.06
HD208313	5055	4.3	-0.05	1			5.2	5.22	5.25	0.02
HD208906	5965	4.2	-0.8	1.7	4.3	4.35			4.25	-0.16
HD210667	5461	4.5	0.15	0.9			5.45	5.45	5.48	0.06
HD210752	6014	4.6	-0.53	1.1	4.65	4.68	4.65	4.58	4.55	-0.11
HD211472	5319	4.4	-0.04	1.1	5.18	5.22	5.17	5.12	5.17	-0.05
HD214683	4747	4.6	-0.46	1.2				4.7	4.65	-0.11
HD216259	4833	4.6	-0.55	0.5				4.45	4.45	-0.24
HD216520	5119	4.4	-0.17	1.4			4.95	5.02	5.02	-0.08
HD217014	5763	4.3	0.17	1.1			5.42	5.42	5.42	0
HD217813	5845	4.3	0.03	1.5	5.2	5.2	5.25	5.17	5.17	-0.09
HD218868	5547	4.45	0.21	0.4			5.52	5.54	5.54	0.07
HD219538	5078	4.5	-0.04	1.1			5.18	5.25	5.25	0.02
HD219623	5949	4.2	0.04	1.2	5.2	5.2	5.18	5.2	5.2	-0.1
HD220140	5144	4.6	-0.03	2.4			5.18	5.18	5.18	-0.04
HD220182	5364	4.5	-0.03	1.2	5.25	5.25	5.25	5.18	5.2	0
HD220221	4868	4.5	0.16	0.5			5.53	5.38	5.45	0.04
HD221851	5184	4.4	-0.09	1			5.07	5.05	5.1	-0.09
HD222143	5823	4.45	0.15	1.1			5.37	5.28	5.32	-0.08
HD224465	5745	4.5	0.08	0.8			5.35	5.3	5.32	-0.01
HD263175	4734	4.5	-0.16	0.5			5.08	5.02	5.02	-0.05
HDBD+12063	4859	4.4	-0.22	0.6			4.85	4.88	4.94	-0.14
HDBD+124499	4678	4.7	0	0.5			5.32	5.25	5.25	0.02
Hercules										
HD13403	5724	4	-0.31	1.1	4.88	4.88	4.93	4.9	4.9	-0.05
HD19308	5844	4.3	0.08	1.1			5.44	5.36	5.36	0.06
HD23050	5929	4.4	-0.36	1.1	4.87	4.85	4.87	4.8	4.77	-0.07
HD30562	5859	4	0.18	1.1			5.44	5.41	5.44	0
HD64606	5250	4.2	-0.91	0.8	4.26	4.26	4.28	4.2	4.2	-0.11
HD68017	5651	4.2	-0.42	1.1	4.78	4.78	4.83	4.73	4.73	-0.07
HD81809	5782	4	-0.28	1.3	4.85	4.85	4.92	4.82	4.8	-0.13
HD107213	6156	4.1	0.07	1.6	5.35	5.35	5.35	5.35	5.3	0.01
HD139323	5204	4.6	0.19	0.7			5.65	5.55	5.55	0.14
HD144579	5294	4.1	-0.7	1.3	4.45	4.45	4.53	4.4	4.4	-0.11
HD159222	5834	4.3	0.06	1.2	5.38	5.38	5.37	5.33	5.28	0.03
HD159909	5749	4.1	0.06	1.1	5.36	5.36	5.32	5.28	5.28	0
HD215704	5418	4.2	0.07	1.1			5.38	5.32	5.32	0.02
HD218209	5705	4.5	-0.43	1	4.75	4.75	4.79	4.72	4.69	-0.09
HD221354	5242	4.1	-0.06	1.2			5.2	5.2	5.2	0.01
Nonclass										
HD4628	4905	4.6	-0.36	0.5			4.8	4.8	4.8	-0.09
HD4635	5103	4.4	0.07	0.8			5.4	5.35	5.35	0.05
HD10145	5673	4.4	-0.01	1.1	5.18	5.18	5.22	5.15	5.15	-0.07
HD12051	5458	4.55	0.24	0.5			5.5	5.5	5.5	0.01
HD13974	5590	3.8	-0.49	1.1	4.7	4.7	4.7	4.65	4.65	-0.09
HD17660	4713	4.75	0.17	1.3			5.55	5.5	5.5	0.1
HD20165	5145	4.4	-0.08	1.1			5.18	5.15	5.15	-0.01
HD24206	5633	4.5	-0.08	1.1	5.2	5.18	5.18	5.12	5.1	-0.02
HD32147	4945	4.4	0.13	1.1			5.5	5.45	5.45	0.09

Table 1: Continued.

Star	$T_{\text{eff},\text{K}}$	$\log g$	Vt	[Fe/H]	4783, A	4823,A	5432,A	6013,A	6021, A	[Mn/Fe]
HD45067	6058	4	-0.02	1.2	5.2	5.2	5.17	5.1	5.1	-0.09
HD84035	4808	4.8	0.25	0.5			5.7	5.62	5.62	0.15
HD86728	5725	4.3	0.22	0.9			5.5	5.5	5.5	0.03
HD90875	4788	4.5	0.24	0.5			5.72	5.62	5.62	0.14
HD117176	5611	4	-0.03	1	5.22	5.25	5.25	5.18	5.18	-0.01
HD117635	5230	4.3	-0.46	0.7			4.75	4.7	4.7	-0.07
HD154931	5910	4	-0.1	1.1	5.17	5.18	5.18	5.1	5.1	-0.01
HD159482	5620	4.1	-0.89	1	4.2	4.2		4.12	4.12	-0.21
HD168009	5826	4.1	-0.01	1.1	5.3	5.3	5.3	5.25	5.22	0.02
HD173701	5423	4.4	0.18	1.1			5.58	5.52	5.52	0.11
HD182736	5430	3.7	-0.06	1	5.26	5.26	5.28	5.16	5.16	0.02
HD184499	5750	4	-0.64	1.5	4.5	4.5	4.5	4.45	4.45	-0.14
HD184768	5713	4.2	-0.07	1.1	5.2	5.2	5.2	5.15	5.15	-0.01
HD186104	5753	4.2	0.05	1.1	5.38	5.38		5.3	5.3	0.03
HD215065	5726	4	-0.43	1.1	4.75	4.75		4.65	4.65	-0.13
HD219134	4900	4.2	0.05	0.8			5.39	5.35	5.39	0.08
HD219396	5733	4	-0.1	1.2	5.12	5.14		5.03	4.98	-0.09
HD224930	5300	4.1	-0.91	0.7	4.2	4.2	4.1	4.1	4.1	-0.21

This paper has been typeset from a $\text{\TeX}/\text{\LaTeX}$ file prepared by the author.